Terahertz scale microbunching instability driven by high resistivity nonevaporable getter coating resistive-wall impedance

Weiwei Li, Tianlong He,* and Zhenghe Bai

National Synchrotron Radiation Laboratory, University of Science and Technology of China, Hefei, Anhui 230029, China

(Received 11 August 2023; revised 4 December 2023; accepted 20 February 2024; published 6 March 2024)

Nonevaporable getter (NEG) coating is widely required in the new generation of light sources and circular e^+e^- colliders for small vacuum pipes to improve the vacuum level, which, however, also enhances the high-frequency resistive-wall impedance and often generates a resonator-like peak in the terahertz frequency region. In this paper, we will use the parameters of the planned Hefei Advanced Light Facility storage ring to study the impact of NEG-coating resistive-wall impedance on the longitudinal microwave instability via particle tracking simulation. Using different NEG-coating parameters (resistivity and thickness) as examples, we find that the impedance with a narrow and strong peak in the terahertz frequency region can cause terahertz scale microbunching instability, which has a low instability threshold current and contributes to a large energy spread widening above the threshold. In order to obtain a convergent simulation of the beam dynamics, one must properly resolve such a peak. The coating with a lower resistivity has a less sharp peak in its impedance spectrum, and there is a regime that it is helpful to suppress the terahertz scale microbunching instability and in return contributes to a higher instability threshold current.

DOI: 10.1103/PhysRevAccelBeams.27.034401

I. INTRODUCTION

The nonevaporable getter (NEG) coating [1] has been successfully applied to inner surfaces of many vacuum chambers of particle accelerators. It can provide distributed pumping along the vacuum chambers, and thus the specified ultrahigh vacuum pressure level could be met with a reduced number and a size of external pumps.

The resistivity wall (RW) impedance, produced by the finite conductivity of the beam vacuum chamber, plays an important, often dominant, role in modern accelerators, especially in those with a small transverse size of the vacuum chamber [2,3]. The presence of the NEG-coating films makes the surface resistance of the beam pipe higher than the one without coating, and the resistive wall effect is more pronounced. This impact is especially important for large machines with small beam pipe dimensions such as circular e^+e^- colliders [4,5] and diffraction-limited storage rings (DLSRs) [6–8]. In addition, there could be also an uncertainty on the coating conductivity measurements in the high frequency region, which may give inaccurate predictions about the instability threshold. In order to reduce the RW impedance contribution and the uncertainty due to the mostly unknown coating resistivity, one of the best ways is to reduce the NEG-coating thickness. Several DLSR projects [6–8] have set the NEG-coating thickness targets equal to or less than 1 μm. A recent study [8] also shows that there is a regime, in which a coating with a lower resistivity produces even a larger loss factor than that with a higher resistivity.

The RW has a strong longitudinal impedance in the high-frequency region, contributing to a sharp variation of the point-charge longitudinal wakefield in very short distances. The presence of the NEG coating will further enhance the high-frequency impedance and often generate a resonator-like peak in the terahertz region [8–10].

The multiparticle tracking simulations [11–14] are widely used to study the beam dynamics but may have computational issues in studying the longitudinal microwave instability (MWI), where a large number of simulation particles is needed to study the response of small-scale bunch structures to high-frequency wakefield components. If not equipped with suitable algorithms (i.e., smoothing/filtering techniques, fine grids, etc.), the simulation can fail to produce reliable results [15]. Since the collective behavior usually does not depend on the behavior of the wakefield/impedance at very small length scales/very high frequencies, one popular solution is to use the wake potential of a very short Gaussian bunch of rms length $\bar{\sigma}_s$

*htlong@ustc.edu.cn

TABLE I. Main parameters of the vacuum chambers.

Type	Material + film (thickness: μm)	Shape	Aperture/radii (mm)	Length (m)
Main chamber	CuCrZr + NEG (d)	Round	13	344.2
Fast corrector	Inconel + NEG (d)	Round	13	7.2
Beam pipes with antechamber	Stainless steel + Cu (20)	Round	13	48.2
Out vacuum insertion devices	Al	Elliptical	$26(H) \times 8(V)$	43
In-vacuum undulators	NdFeB + Ni (75) + Cu (75)	Rectangular	$65(H) \times 6(V)$	5.4
Others (i.e., bellows and flanges)	Stainless steel	Round	13	32

(sometimes called pseudo-Green function) in place of the point-charge wakefield [3]. Then the impedance used in tracking simulation becomes that of the point-charge multiplied by a Gaussian filter. The remaining item is to determine the required length $\bar{\sigma}_s$, which effectively means that finding the frequency range over which the impedance affects the dynamics. Usually, the guideline $\bar{\sigma}_s \cong \frac{1}{10}\sigma_{z0}$ or $\frac{1}{15}\sigma_{z0}$ gives a reasonable estimate [3], where σ_{z0} is the equilibrium rms beam length at zero current limit. This guideline or even longer $\bar{\sigma}_s$ is also widely used nowadays when dealing with the NEG-coating RW [4,16,17]. In general, the MWI simulations are quite sensitive to numerical noise, so it is necessary to vary different tracking parameters to make sure that the tracking results are convergent.

In the Hefei Advanced Light Facility (HALF) project [18], a fourth generation light source in design, studying the impact of the NEG-coating parameters on the beam dynamics is also necessary. At first, we also adopted the guideline that $\bar{\sigma}_s \cong \frac{1}{10}\sigma_{z0}$ in the tracking simulations, where $\sigma_{z0} = 2.1$ mm for HALF. However, in doing so, the wake forces corresponding to the high-frequency impedance components in the terahertz region would also be filtered out (as will be seen in Fig. 3) and we were in doubt as to whether it is reasonable to ignore the impact of such strong impedance components on the beam dynamics even if their frequencies are very high. So we try to vary $\bar{\sigma}_s$ as well in order to obtain a quasiconvergent tracking simulation and find the required length $\bar{\sigma}_s$ should typically be even smaller than 0.02 mm, meanwhile very tiny grid/bin size and a large number of macroparticles are necessary. Under convergent simulations, we discover that the coating with a high resistivity (in the order of 10^{-5} Ωm), whose impedance has a sharp peak in the terahertz region, can cause an undesirable terahertz scale microbunching instability (MBI), with a low threshold current and a large energy spread widening.

This paper is organized as follows: In Sec. II, the RW impedance with different NEG-coating parameters of HALF will be presented. In Sec. III, the particle tracking method will be introduced. Section IV shows the simulation results with only RW impedance using different tracking and coating parameters. The conclusions and discussions are presented in Sec. V. As an extension, the Appendix shows the simulation results with CSR impedance taken into consideration as well.

II. RESISTIVE WALL IMPEDANCE IN HALF

We consider a simplified model of the ring consisting of six parts and the main parameters of the vacuum chambers are listed in Table I, where symbols H and V are short for horizontal and vertical sizes, respectively. The direct current (dc) resistivities of the materials are listed in Table II.

The NEG-resistivity value depends on the compound composition and coating method [19]. The resistivity measurement results also have very large discrepancy using different methods [20]. Thus three different resistivity ρ_{NEG} values will be taken into account: 1×10^{-5}, 5×10^{-6}, and 1×10^{-6} Ωm. The target of NEG-coating thickness is $d = 1$ μm for the HALF project, but two different film thicknesses will be studied for comparison: 0.5 and 1 μm.

The resistive wall impedance is computed using the IMPEDANCEWAKE2D (IW2D) code [21], which solves for a circular geometry and then applies a Yokoya factor for elliptical or rectangular cases [22,23]. The frequency dependent resistivities are obtained by the Drude model in IW2D. The total longitudinal impedance as a function of frequency is shown in Fig. 1. At low frequency, all the impedance is similar since the thickness of the coating is much smaller than its skin depth. At high frequency, the impedance is greatly enhanced with NEG coatings and generates a resonator-like peak in the terahertz region. If the coating resistivity or thickness is smaller, the impedance will be more close to that of no coating. A smaller coating resistivity will reduce the quality factor and the peak

TABLE II. dc resistivities of the materials.

Material	Resistivity (Ωm)
Cu	1.68×10^{-8}
CuCrZr	2.3×10^{-8}
Al6063	3.16×10^{-8}
Ni	6.93×10^{-7}
SS316L	7.41×10^{-7}
Inconel 625	1.29×10^{-6}

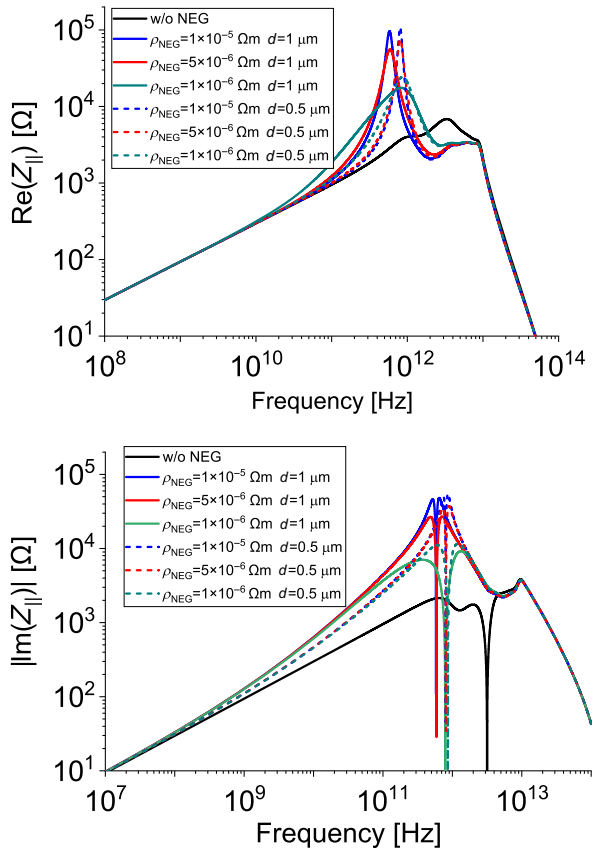

FIG. 1. Real (top) and the absolute value of the imagine (bottom) parts of the longitudinal impedance for different coating parameters.

impedance. A thinner coating thickness will make the peak frequency shift downward.

It is useful to define the effective impedance as [24–26]

$$\left(\frac{Z_\parallel}{n}\right)_{\text{eff}} = \frac{\int_{-\infty}^{\infty} Z_\parallel(\omega)\frac{\omega_0}{\omega}h(\omega)d\omega}{\int_{-\infty}^{\infty} h(\omega)d\omega}, \tag{1}$$

where $n = \omega/\omega_0$ is the revolution harmonic number, ω_0 is the revolution angular frequency, $h(\omega) = \tilde{\lambda}(\omega)\tilde{\lambda}^*(\omega)$ is the bunch power spectrum, $\tilde{\lambda}(\omega)$ is the Fourier transform of the longitudinal charge density $\lambda(t)$. Assuming a Gaussian bunch, $h(\omega) = e^{-\omega^2\sigma_t^2}$, where σ_t is the rms bunch length in time. The effective impedance with natural bunch length (7 ps) for different NEG-coating parameters are listed in Table III.

TABLE III. Effective impedance (mΩ) with natural bunch length for different NEG-coating parameters.

	ρ_{NEG}(Ωm)		
d (μm)	1×10^{-5}	5×10^{-6}	1×10^{-6}
1	77.7	77.5	76.5
0.5	67.2	67.1	66.6

III. MULTIPARTICLE TRACKING SIMULATION

Most of the macroparticle tracking codes compute the wake potential as the convolution between the longitudinal wake function $w_\parallel(t)$, i.e., the Green function of a point charge and the bunch distribution $\lambda(t)$: [12]

$$W_\parallel(t) = \int_{-\infty}^{t} w_\parallel(t-t')\lambda(t')\mathrm{d}t'. \tag{2}$$

The longitudinal wake function can be expressed in terms of the longitudinal impedance by an inverse Fourier transform:

$$w_\parallel(t) = \frac{1}{2\pi}\int_{-\infty}^{\infty} Z_\parallel(\omega)e^{i\omega t}d\omega. \tag{3}$$

For the convenience of numerical calculation, the time coordinate in Eq. (2) should be equispaced and discrete Fourier transforms can be used. The bin size is $\Delta_t = \frac{0.5}{F_m}$, where F_m is the maximum frequency of the impedance in Eq. (3). $\lambda(t)$ is obtained by counting the particle number in each bin and $> \sim$1000 particles per bin is typically required. However, the input RW wake function can cause some problems to simulations based on this approach, since it covers a very high-frequency range and a very large number of slices would be necessary, thus increasing the computational load. As discussed in Sec. I, the pseudo-Green function from a very short Gaussian pulse will be used. The pulse length $\bar{\sigma}_s$ will determine the frequency reach of the impedance calculation and needs to be much smaller than the real bunch length used in tracking simulations to cover the spectrum of interest. However, in order to resolve the impedance peak, the computational load is still very heavy.

The STABLE code [27] will be dedicated to conduct multiparticle tracking simulations for longitudinal beam dynamics studies. It is implemented in a MATLAB environment with the usage of the state-of-the-art of graphics-processing-unit acceleration technique so that the tracking efficiency is significantly improved. The original version of STABLE is written for multibunch and multiparticle simulation, and a 2D matrix is used to store the macroparticle's coordinates, with each column corresponding to one bunch. In order to accurately simulate the single bunch dynamics, which usually requires millions or even tens of millions of macroparticles, we need only modify the STABLE code by dividing the macroparticles of a single bunch into multiple parts and storing them in each column of the 2D matrix. We can separately count the bin distribution of each column and then summarize them to obtain the total bunch distribution. In addition, a fixed bin width instead of the number of bins is set in default. Therefore, the bin number

will increase as the bunch lengthening. The remaining operations, such as convolution of the bunch distribution and the short-range wake (or short-bunch wakepotential), and interpolation to obtain the short-range wake kick of each macroparticle, can be the same as those in the original version of STABLE.

IV. NUMERICAL RESULTS FOR THE PARAMETERS OF HALF

In this section, the impact of NEG-coated resistive-wall impedance on the longitudinal beam dynamics is investigated by tracking simulations in the framework of the HALF project. The main parameters of the HALF storage ring with insertion devices are summarized in Table IV. We expect about 10% empty buckets are necessary to suppress the ion effects [28], and then the single bunch current is about 0.49 mA.

A. Convergence study

We first carry out the convergence study with two typical examples, the coatings with $\rho_{\mathrm{NEG}} = 1 \times 10^{-5}$ Ωm, $d = 1$ μm and $\rho_{\mathrm{NEG}} = 1 \times 10^{-6}$ Ωm, $d = 1$ μm, respectively.

1. Pseudo-Green function

The wake potentials for the short Gaussian bunch of $\bar{\sigma}_s = 0.1$ and 0.01 mm are shown in Fig. 2, where the positive (negative) value means energy loss (gain), and they will be used instead of the wake function generated from a point charge. To calculate the effective impedance or loss factors for a perfect Gaussian bunch distribution with nominal bunch length σ_{t0} from the pseudo-Green function, using the wake potentials of $\bar{\sigma}_s = 0.1$ mm can usually obtain sufficiently accurate results. Note that $\bar{\sigma}_s = 0.1$ mm is more than 20 times shorter than the natural bunch length σ_{t0}.

The longitudinal impedance multiplied by the Fourier spectrum $\tilde{\lambda}(\omega)$ of the Gaussian bunches with different $\bar{\sigma}_s$ is plotted in Fig. 3. In order to resolve the impedance peak clearly, $\bar{\sigma}_s$ should be smaller than 0.02 mm.

TABLE IV. Main parameters of HALF.

Parameter	Symbol	Value
Ring circumference	C	480 m
Beam energy	E_0	2.2 GeV
Nominal beam current	I_0	350 mA
Longitudinal damping time	τ_z	14 ms
Momentum compaction	α_c	9.4×10^{-5}
Natural energy spread	σ_δ	7.3×10^{-4}
Harmonic number	h	800
Energy loss per turn	U_0	400 keV
Voltage of MC	V_{rf}	1.2 MV
Natural rms bunch length	σ_{t0}	7 ps

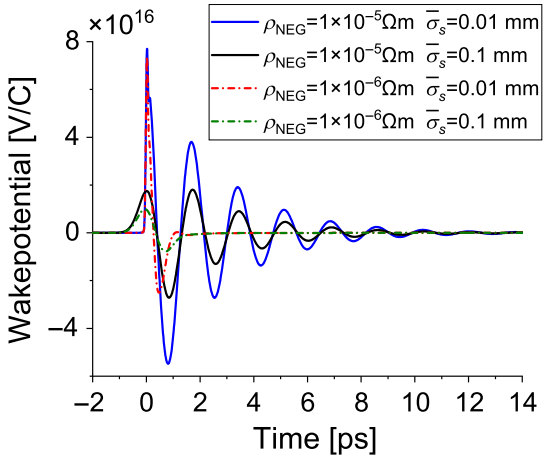

FIG. 2. Longitudinal wake potentials for different ρ_{NEG} and $\bar{\sigma}_s$. The coating thickness is $d = 1$ μm.

2. The case for $\rho_{\mathrm{NEG}} = 1 \times 10^{-5}$ Ωm and $d = 1$ μm

Figure 4 shows the predicted energy spread and bunch lengthening from the tracking simulations as a function of

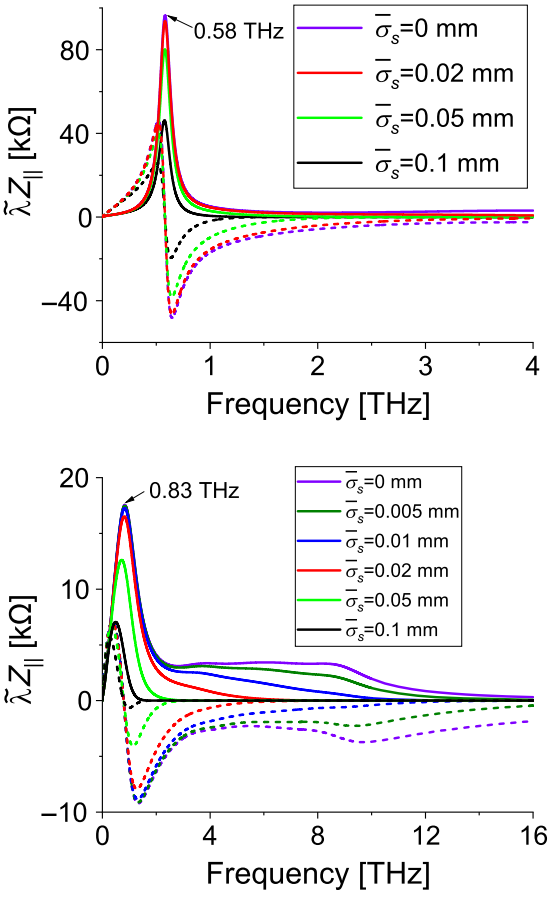

FIG. 3. Real (solid) and imagined (dashed) parts of the longitudinal impedance multiplied by different Gaussian filters for $\rho_{\mathrm{NEG}} = 1 \times 10^{-5}$ Ωm (top) and $\rho_{\mathrm{NEG}} = 1 \times 10^{-6}$ Ωm (bottom). The coating thickness is $d = 1$ μm.

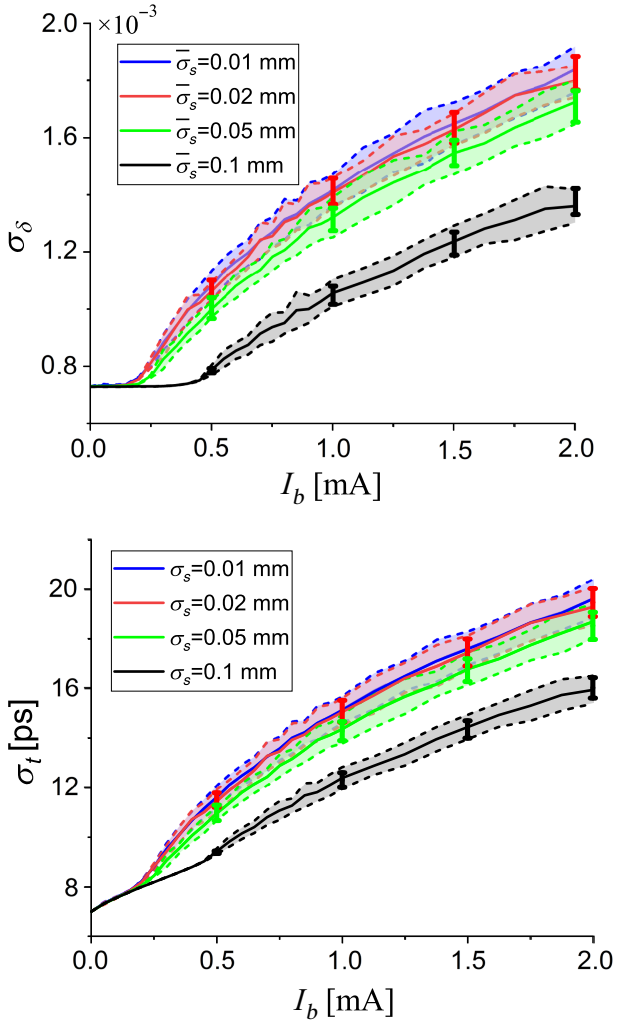

FIG. 4. The rms energy spread (top) and bunch length (bottom) versus single bunch current for $\rho_{\mathrm{NEG}} = 1 \times 10^{-5}$ Ωm and $d = 1$ μm with different $\bar{\sigma}_s$. The solid lines are the mean values and the dashed lines including their fill areas represent the standard deviation obtained by STABLE with current the step of 0.05 mA. The discrete error bars are obtained by PELEGANT with the current step of 0.5 mA.

the single bunch current for $\rho_{\mathrm{NEG}} = 1 \times 10^{-5}$ Ωm and $d = 1$ μm with various values of $\bar{\sigma}_s$, where the particle number N_p is 5 million (M), 40 000 turns are tracked for each current, and the bin size Δ_t is set to be 0.02 ps. The corresponding F_m is 25 THz, which should be high enough to cover the frequency region of interest. Another guideline is that Δ_t should be small enough to resolve the wake potential generated from the short Gaussian bunch with $\bar{\sigma}_s$. The mean value and standard deviation of bunch length and relative energy spread are computed on the last 10 000 turns. To benchmark the simulation results from the STABLE code, the PELEGANT code [29] is also used with the same parameters except for fewer current and $\bar{\sigma}_s$ values, and the results are also marked in Fig. 4. In order to obtain one data point in Fig. 4, it takes about 200 min for PELEGANT using

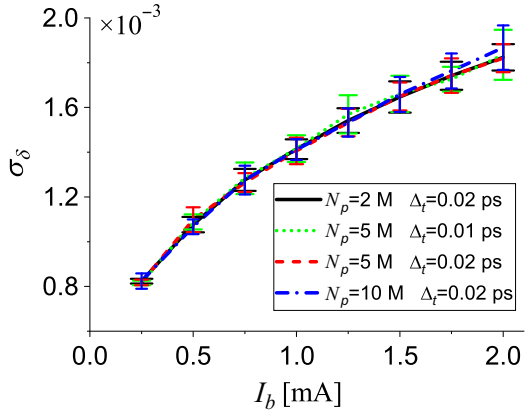

FIG. 5. Energy spread versus single bunch current for $\rho_{\mathrm{NEG}} = 1 \times 10^{-5}$ Ωm and $d = 1$ μm $\bar{\sigma}_s = 0.01$ mm with different N_p and Δ_t. The lines represent the mean values and the error bars represent the standard deviation.

80 CPU cores, while less than 10 min for STABLE using 3584 CUDA cores. Good agreements are achieved since their underlying physical models are the same. Thus we will only use the STABLE code for the other simulations.

To validate the choice of the bin size Δ_t and the particle number N_p, convergence studies are performed for the case of $\bar{\sigma}_s = 0.01$ mm, since a shorter $\bar{\sigma}_s$ requires more severe convergence conditions. The corresponding energy spreads are shown in Fig. 5. There is no significant variation when Δ_t decreases from 0.02 to 0.01 ps or N_p varies from 2 to 10 M.

As seen in Fig. 4, at the low current below the MWI threshold, the simulations using a relatively long $\bar{\sigma}_s = 0.1$ mm have already given enough convergent results. However, in order to accurately evaluate the MWI, one must properly resolve the resonator-like peak impedance. To obtain a full convergent simulation for the coating with $\rho_{\mathrm{NEG}} = 1 \times 10^{-5}$ Ωm and $d = 1$ μm, the required $\bar{\sigma}_s$ is 0.02 mm. The MWI behavior can be significantly underestimated if the wakefield resolution $\bar{\sigma}_s$ is not sufficient.

3. *The case for $\rho_{\mathrm{NEG}} = 1 \times 10^{-6}$ Ωm and $d = 1$ μm*

Figure 6 shows the predicted energy spread from the tracking simulations as a function of the single bunch current for $\rho_{\mathrm{NEG}} = 1 \times 10^{-6}$ Ωm and $d = 1$ μm with various values of $\bar{\sigma}_s$ and N_p, where $\Delta_t = 0.02$ ps and the current step is 0.25 mA. For $\bar{\sigma}_s = 0.1$ mm, if $N_p = 2$ M is adopted, it shows obvious energy spread widening, but as with the increment of N_p, the energy spread widening becomes smaller and when N_p increases to 50 M, there is nearly no MWI within 2 mA. However, the peak impedance is still not resolved, thus we further study the case of $\bar{\sigma}_s = 0.01$ and 0.005 mm. With the same N_p, their results are close, so $\bar{\sigma}_s = 0.01$ mm should be enough to cover the frequency region of interest. Within 1.5 mA, the energy

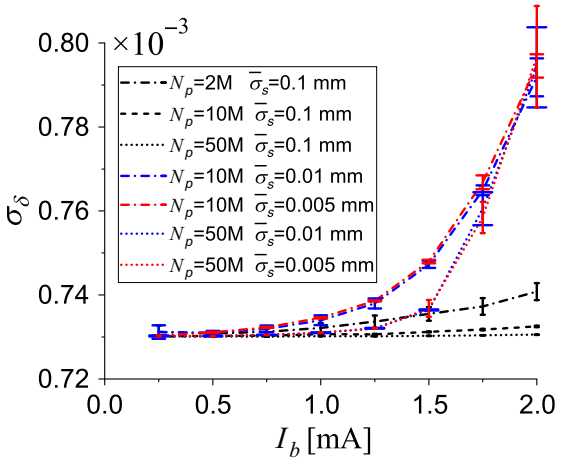

FIG. 6. rms energy spread versus single bunch current for $\rho_{\mathrm{NEG}} = 1 \times 10^{-6}$ Ωm and $d = 1$ μm with different N_p and $\bar{\sigma}_s$. The lines represent the mean values and the error bars represent the standard deviation.

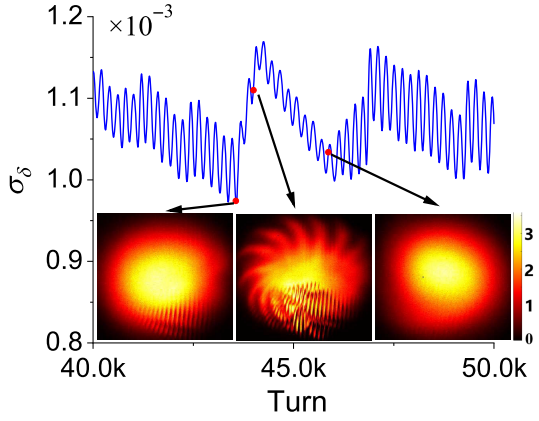

FIG. 7. rms energy spread evolution over the pass turn for $\rho_{\mathrm{NEG}} = 1 \times 10^{-5}$ Ωm and $d = 1$ μm at 0.5 mA together with the longitudinal phase space plots $(t - \delta)$ at three marked points.

spread widening becomes smaller as with the increment of N_p, but the full convergence is still not achieved even when $N_p = 50$ M. Anyway, the energy spread widening remains relative small. Therefore, we can conclude that there is no or very weak MWI within 1.5 mA, and it is reasonable to use a long $\bar{\sigma}_s$ such as 0.1 mm to filter out the high-frequency wakefield components. For $\bar{\sigma}_s = 0.01$ or 0.005 mm at a high current of 2 mA, there is no significant variation when N_p varies from 10 to 50 M, and the obvious energy spread widening can be seen, so in this situation, one should also use a small $\bar{\sigma}_s$ to resolve the resonator-like peak impedance in order to accurately predict the MWI behavior.

B. Microbunching instability phenomena

In the previous section, it was shown that the coating with $\rho_{\mathrm{NEG}} = 1 \times 10^{-5}$ Ωm and $d = 1$ μm causes a much more serious MWI than that with $\rho_{\mathrm{NEG}} = 1 \times 10^{-6}$ Ωm and $d = 1$ μm although they are close in effective impedance with natural bunch length, so there is a practical interest in exploring the underlying mechanism.

The energy spread evolution over the pass turn for $\rho_{\mathrm{NEG}} = 1 \times 10^{-5}$ Ωm and $d = 1$ μm with $\bar{\sigma}_s = 0.01$ mm and $N_p = 20$ M at a current of 0.5 mA together with the longitudinal phase space distributions at three different turns are shown in Fig. 7, where the bunch head is on the left, and the color bar represents the charge density with the arbitrary unit. More simulated particles are used just to make the plots of the phase spaces more smooth and clear. There appear strong sawtooth-shaped fluctuations of energy spread over the pass turn. The error bars in Figs. 4 and 5 also characterize the amplitudes of the fluctuations. The MBI in the phase space is visible, and the bunching frequency happens to be around that of the peaked impedance (0.58 THz, as marked in Fig. 3). It implies that the sharp peak in the impedance spectrum plays an important role in the MBI. A possible reason is that when the peak is narrowband (or has a high-quality factor), the corresponding wakefield lasts for several oscillation cycles (as shown in Fig. 2), which allows the wakefield from the microbunches far apart to be coherently enhanced. While for $\rho_{\mathrm{NEG}} = 1 \times 10^{-6}$ Ωm and $d = 1$ μm, the peak is more broadband, the wakefield attenuates quickly with the increasing distance, which prevents the cooperation between the microbunching fluctuations far apart.

In order to resolve such tiny microstructures in the phase space, it also requires very small Δ_t and great N_p. As for a rough estimate, the bunching frequency is about 0.5 THz and the bin size should typically be at most $1/10$ of the bunching interval, and then Δ_t should be smaller than 0.2 ps. The total bunch length should typically be at least 6 times of σ_{t0} (7 ps for HALF), so it needs at least 200 bins to cover the beam region and millions of particles to ensure $> \sim 1000$ particles per bin. From this point of view, our choice of $\Delta_t = 0.02$ ps is also sufficient.

C. Impact of coating parameters

We have shown the coating with $\rho_{\mathrm{NEG}} = 1 \times 10^{-5}$ Ωm and $d = 1$ μm can cause the MBI effect with a low current threshold for the HALF ring. To avoid its occurrence, there is a practical interest in exploring the dependence on the coating parameters.

We consider the coating parameters given in Sec. II, in which their impedances are given. Figure 8 shows the predicted energy spread and bunch lengthening from the tracking simulations as a function of the single bunch current for different coating parameters, where the current step is 0.25 mA, $\Delta_t = 0.02$ ps, and $\bar{\sigma}_s = 0.01$ mm, which is small enough to resolve the resonator-like peak impedance, and the particle number is 10 M except for the case of

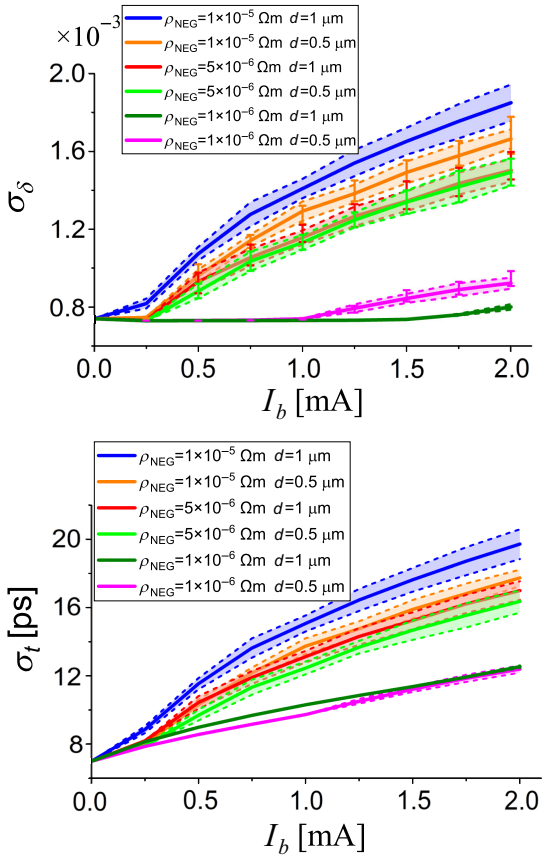

FIG. 8. rms energy spread (top) and bunch length (bottom) versus single bunch current for different coatings. The solid lines are the mean values and the dashed lines including their fill areas represent the standard deviation. The discrete error bars are obtained using $N_p = 20$ M to validate the convergences.

$\rho_{\mathrm{NEG}} = 1 \times 10^{-6}$ Ωm and $d = 1$ μm, where 50 M particles are used. The convergence studies for the cases $\rho_{\mathrm{NEG}} = 1 \times 10^{-5}$ Ωm, $d = 1$ μm and $\rho_{\mathrm{NEG}} = 1 \times 10^{-6}$ Ωm, $d = 1$ μm have been done in Sec. IV A. To validate the choice of N_p for the other cases, we also carry out the simulations using $N_p = 20$ M and the results are also plotted in Fig. 8 as error bars, and there is no significant variation for each case. With the same coating thickness $d = 1$ or 0.5 μm, the MWI for $\rho_{\mathrm{NEG}} = 5 \times 10^{-6}$ Ωm is less serious and has a higher threshold current than that for $\rho_{\mathrm{NEG}} = 1 \times 10^{-5}$ Ωm, but there still exits terahertz scale MBI when the current exceeds the threshold. For the coating with resistivity $\rho_{\mathrm{NEG}} = 1 \times 10^{-5}$ Ωm or 5×10^{-6} Ωm, reducing the thickness from 1 down to 0.5 μm is helpful to weaken the MBI since the peak frequency in the impedance spectrum for $d = 0.5$ μm is higher than that for $d = 1$ μm as seen in Fig. 1. For the coating with $\rho_{\mathrm{NEG}} = 1 \times 10^{-6}$ Ωm and $d = 1$ μm, it does not contribute to terahertz scale MBI, so it has a much higher instability threshold and smaller energy spread widening. For the coating with $\rho_{\mathrm{NEG}} = 1 \times 10^{-6}$ Ωm, reducing the coating thickness from 1 down to 0.5 μm will make a lower instability threshold, this is because the impedance peak of the latter is much sharper as shown in Fig. 1, which can also lead to terahertz scale MBI.

D. Impact of bunch lengthening with HHC

Bunch lengthening with higher harmonic cavities (HHCs) is also a very helpful means to fight against most collective effects, including the MWI. A passive superconducting third harmonic cavity will be installed in the HALF storage ring [30,31]. Instead of multibunch simulations, we just carry out single bunch simulations by introducing an ideal HHC voltage potential because of the heavy computational loads and making the bunch length increase to a factor of 2 or 3 at zero current. Figure 9 shows

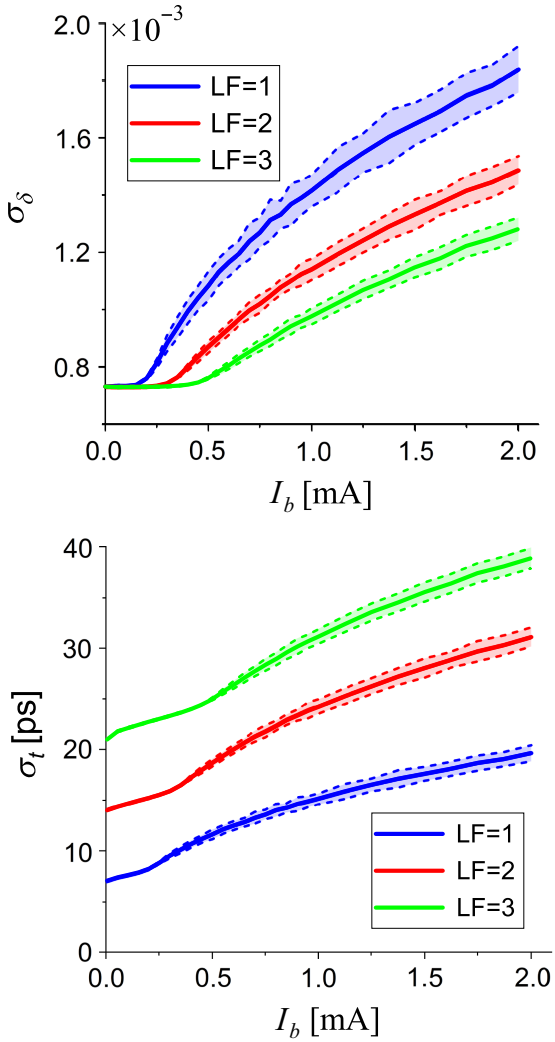

FIG. 9. rms energy spread (top) and bunch length (bottom) versus single bunch current for $\rho_{\mathrm{NEG}} = 1 \times 10^{-5}$ Ωm and $d = 1$ μm with different bunch lengthening factors (LFs). The solid lines are the mean values and the dashed lines including their fill areas represent the standard deviation.

the predicted energy spread and bunch lengthening from the tracking simulations as a function of the single bunch current for the case of $\rho_{\mathrm{NEG}} = 1 \times 10^{-5}$ Ωm and $d = 1$ μm with different bunch lengthening factors. In order to obtain a convergent simulation, $\bar{\sigma}_s$ should still be as small as that without HHC to resolve the resonator-like peak impedance. The bunch lengthening with HHC can raise the MBI/MWI threshold since it lowers the charge density. In this coating case for HALF, the threshold current with the bunch lengthening to a factor of 3 happens to be around the single bunch target of 0.49 mA.

V. CONCLUSION AND DISCUSSION

In this paper, we have studied the impact of NEG-coating resistive-wall (RW) impedance on the longitudinal microwave instability (MWI) for the HALF storage ring via particle tracking simulation, where the wake potential of a very short Gaussian bunch with rms length of $\bar{\sigma}_s$ serves as pseudo-Green function. In order to obtain a quasiconvergent simulation of the beam dynamics, $\bar{\sigma}_s$ should be small sufficiently to resolve the peak impedance in the terahertz region. For the cases presented in this paper, $\bar{\sigma}_s$ should be at most 0.02 mm, which is more than 100 times shorter than that of the equilibrium beam at zero limit. Otherwise, one is likely to underestimate the MWI behavior.

Our MWI studies for HALF show that the characteristics of the peak in the terahertz region are very critical to beam dynamics. A strong and narrowband peak can cause an undesirable terahertz scale microbunching instability (MBI), which has a low threshold current and makes the dynamics of MWI more complex. For the cases of a high coating resistivity of 10^{-5} Ωm, reducing the thickness from 1 to 0.5 μm is helpful to weaken the MBI by shifting the peak impedance to higher frequency, but the MBI is still dangerous. For the cases of coating thickness of 1 or 0.5 μm, reducing the coating resistivity from 1×10^{-5} to 1×10^{-6} Ωm is an effective way to suppress the MBI since the impedance peak becomes broader. We also notice that the MWIs with columnar NEG coating (which has a high resistivity of 7.1×10^{-5} Ωm) were much less serious in Ref. [8], and we infer the reason is that there were only 100 bins in their tracking simulations except for the Appendix, which is not enough to resolve the tiny structures of the terahertz scale MBI (as analyzed in the last paragraph of Sec. IV B).

The bunch lengthening with HHC can raise the MWI/MBI threshold. A storage ring with NEG coating of high resistivity applied to inner surfaces of many vacuum chambers, and a low-frequency main cavity [32,33] can still suffer from the MBI since it has high single bunch charges.

In this paper, the coating parameters are assumed to be constant along the ring; however, there is always spread in the coating parameters in the real machine. The spread will broaden the impedance peak and weaken the terahertz scale MBI. The NEG-coating RW impedance in the terahertz frequency region can play an important role in the MBI, so accurate measurements of the coating parameters, including the resistivity in the terahertz frequency region, thickness, and their spreads, are very important in order to model the total RW impedance and perform accurate simulations on their impact on the beam dynamics. We would like to measure the coating parameters by ourselves or cooperate with other laboratories in the future. Our vacuum technology group has also developed an approach to reduce the coating resistivity by adding copper to NEG-film composition [34] and is now also making an effort to reduce the part of the HALF main vacuum chamber with NEG coating as much as possible, say $1/3$, in order to reduce the RW impedance and the uncertainty due to the mostly unknown coating resistivity.

The MBI will degrade the beam quality but also has the potential to tailor the emitted CSR radiation and its fluctuations for possible applications of the terahertz radiation. However, it should be based on accurate measurements of the NEG-coating parameters so that one can predict the beam dynamics accurately during the machine design. Under normal operations of the storage ring, one should avoid MBI. While for terahertz users, one can make the MBI occur by less bunch lengthening with harmonic cavity or increasing single bunch charges with less filled buckets.

ACKNOWLEDGMENTS

The authors would like to thank Sihui Wang at USTC and Na Wang at IHEP for the useful discussions on NEG coatings and Biaobin Li at USTC for useful discussions on the numerical convergence. This work was supported by the National Natural Science Foundation of China (Grants No. 12341501, No. 12375324, No. 12375325, No. 12105284, and No. 11875259) and the Fundamental Research Funds for the Central Universities (Grant No. WK2310000090).

APPENDIX: NUMERICAL RESULTS WITH CSR AS WELL

For HALF, CSR is also a possible MBI driven source, so we will consider it here together with the NEG-coating RW. The impedance and wakefield of CSR using the parallel plates model [35] with full gap of $2h = 26$ mm and the results are shown in Figs. 10 and 11, where those of RW with $\rho_{\mathrm{NEG}} = 1 \times 10^{-5}$ Ωm, 1×10^{-6} Ωm, and $d = 1$ μm are also plotted as comparison. The CSR impedance is broadband and strong in the high-frequency region, and its wakefield is very short. The RW with a high (low) resistivity coating has a narrow (wide) band impedance and long (short) wakefield.

The MBI driven by CSR has been extensively studied elsewhere such as in [36–39], while the terahertz scale MBI

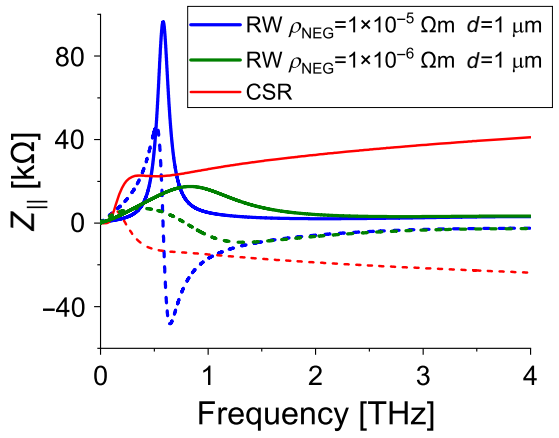

FIG. 10. Real (solid) and imagine (dashed) parts of the longitudinal impedance of NEG-coating RW and CSR.

driven by NEG-coating RW was studied in the text of this paper, so we make a brief comparison between them here. The MBIs induced by them have some common characteristics, such as noise sensibility and the relaxing effect of harmonic cavities, but they also have some differences, for example, the microstructures driven by the NEG-coating RW are bunched around the peak frequency of the impedance and the MBI becomes weaker when its impedance peak becomes broader, while the CSR impedance with parallel plates model is very broadband and the microstructures driven by it do not have a fixed bunching frequency. Anyway, the CSR and NEG-coating RW are the two completely different MBI driven sources.

Figure 12 shows the energy spread and bunch lengthening as a function of a single bunch with different impedance sources, where $\bar{\sigma}_s = 0.02$ mm, $N_p = 20$ M, and $\Delta_t = 0.02$ ps, and we have also validated the convergence by varying them. The MBI driven by CSR and RW with $\rho_{\mathrm{NEG}} = 1 \times 10^{-6}$ Ωm is slightly less serious than that driven by only CSR because of the bunch lengthening caused by RW. The cooperation of CSR and RW with $\rho_{\mathrm{NEG}} = 1 \times 10^{-5}$ Ωm can cause more serious MBI than either of them.

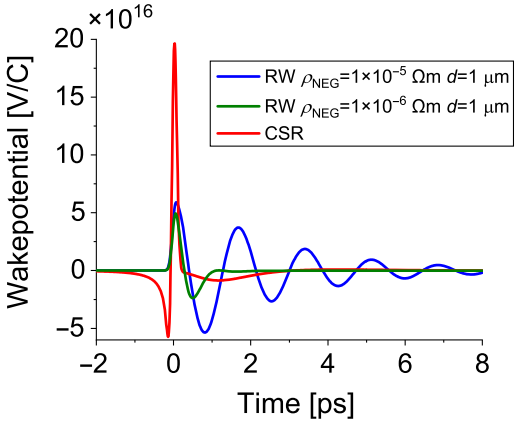

FIG. 11. Longitudinal wake potentials with $\bar{\sigma}_s = 0.02$ mm for NEG-coating RW and CSR.

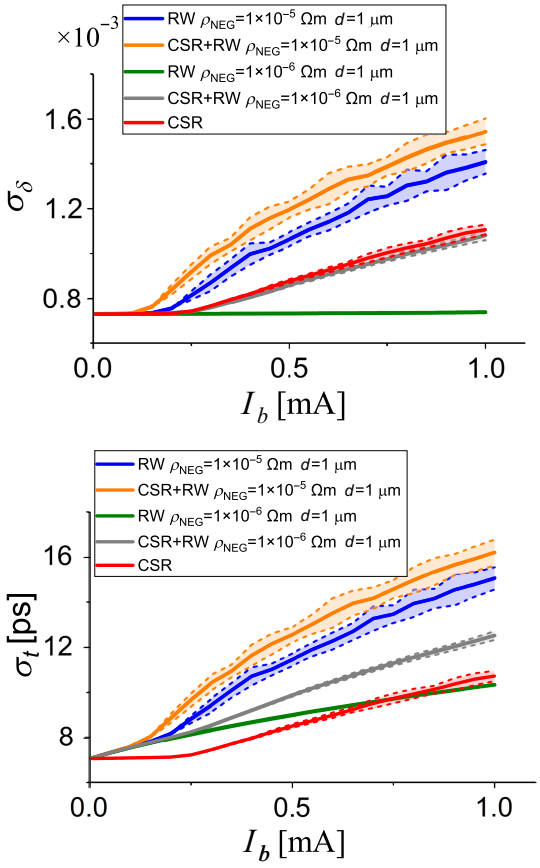

FIG. 12. rms energy spread (top) and bunch length (bottom) versus single bunch current for different coatings. The solid lines are the mean values and the dashed lines including their fill areas represent the standard deviation. The discrete error bars are obtained using $N_p = 20$ M to validate the convergences.

[1] O. B. Malyshev, Nonevaporable getter (NEG)-coated vacuum chamber, in *Vacuum in Particle Accelerators* (John Wiley Sons, Ltd., Hoboken, NJ, 2019), Chap. 5, pp. 175–213.

[2] R. Nagaoka and K. L. F. Bane, Collective effects in a diffraction-limited storage ring, J. Synchrotron Radiat. **21**, 937 (2014).

[3] A. Blednykh, G. Bassi, V. Smaluk, and R. Lindberg, Impedance modeling and its application to the analysis of the collective effect, Phys. Rev. Accel. Beams **24**, 104801 (2021).

[4] M. Migliorati, E. Belli, and M. Zobov, Impact of the resistive wall impedance on beam dynamics in the Future Circular e^+e^- Collider, Phys. Rev. Accel. Beams **21**, 041001 (2018).

[5] N. Wang, C. Lin, Y. Liu, S. Tian, H. Xu, and Y. Zhang, Collective effects studies for CEPC, in *Proceedings of the*

65th ICFA Advanced Beam Dynamics Workshop on High Luminosity Circular e^+e^- Colliders, eeFACT2022, Frascati, Italy (JACoW, Geneva, Switzerland, 2023), WEYAT0101.

[6] N. Wang, Z. Duan, X. Li, H. Shi, S. Tian, and G. Xu, Development of the impedance model in HEPS, in *Proceedings of 8th International Particle Accelerator Conference, IPAC2017, Copenhagen, Denmark* (JACoW, Geneva, Switzerland, 2017), WEPIK078.

[7] M. Dehler *et al.*, Characterization of NEG coatings for SLS 2.0, in *Proceedings of 10th International Particle Accelerator Conference, IPAC2019, Melbourne, Australia* (JACoW, Geneva, Switzerland, 2019), TUPGW108.

[8] A. Gamelin and W. Foosang, Influence of the coating resistivity on beam dynamics, Phys. Rev. Accel. Beams **26**, 054401 (2023).

[9] Y. Shobuda and Y. H. Chin, Resistive-wall impedances of a thin non-evaporable getter coating on a conductive chamber, Prog. Theor. Exp. Phys. **2017**, 123G01 (2017).

[10] S. T. Motlagh, J. Rahighi, F. Zamani, and F. Saeidi, The resistive wall impedance and the effects of the non-evaporable getter thickness in an ultra-low emittance ring, J. Instrum. **18**, P01028 (2023).

[11] https://github.com/PyCOMPLETE/PyHEADTAIL.

[12] G. Skripka, R. Nagaoka, M. Klein, F. Cullinan, and P. F. Tavares, Simultaneous computation of intrabunch and interbunch collective beam motions in storage rings, Nucl. Instrum. Methods Phys. Res., Sect. A **806**, 221 (2016).

[13] H. Xu, U. Locans, A. Adelmann, and L. Stingelin, Calculation of longitudinal collective instabilities with mbtrack-cuda, Nucl. Instrum. Methods Phys. Res., Sect. A **922**, 345 (2019).

[14] L. Wang, J. Yang, M. Chang, and F. Ma, GOAT: A simulation code for high intensity beams, Nucl. Sci. Tech. **34**, 78 (2023).

[15] G. Bassi, A. Blednykh, and V. Smaluk, Self-consistent simulations and analysis of the coupled-bunch instability for arbitrary multibunch configurations, Phys. Rev. Accel. Beams **19**, 024401 (2016).

[16] D. Wang, K. Bane, D. Li, T. Luo, O. Omolayo, G. Penn, S. De Santis, C. Steier, and M. Venturini, Broadband impedance modeling and single bunch instabilities estimations of the advanced light source upgrade project, Nucl. Instrum. Methods Phys. Res., Sect. A **1031**, 166524 (2022).

[17] L. R. Carver, T. Brochard, E. Buratin, N. Carmignani, F. Ewald, L. Hoummi, S. M. Liuzzo, T. Perron, B. Roche, and S. White, Beam based characterization of the European Synchrotron Radiation Facility Extremely Brilliant Source short range wakefield model, Phys. Rev. Accel. Beams **26**, 044402 (2023).

[18] Z. H. Bai, G. Y. Feng, T. L. He, W. Li, W. W. Li, G. Liu, Z. L. Ren, L. Wang, P. H. Yang, S. C. Zhang, and T. Zhang, A modified hybrid 6BA lattice for the HALF storage ring, in *Proceedings of 12th International Particle Accellerator Conference, IPAC2021, Campinas, Brazil* (JACoW, CERN, Genevaa, Switzerland, 2021), MOPAB112.

[19] O. B. Malyshev, L. Gurran, P. Goudket, K. Marinov, S. Wilde, R. Valizadeh, and G. Burt, RF surface resistance study of non-evaporable getter coatings, Nucl. Instrum. Methods Phys. Res., Sect. A **844**, 99 (2017).

[20] E. Plouviez, Comments on resistive measurement of NEG coated surface, in *Proceedings of the 7th Low Emittance Rings Workshop* (CERN, Geneva, Switzerland, 2018).

[21] N. Mounet, ImpedanceWake2D, https://gitlab.cern.ch/IRIS/IW2D.

[22] K. Yokoya, Resistive wall impedance of beam pipes of general cross-section, Part. Accel. **41**, 221 (1993), https://inspirehep.net/files/9d1ce4331167887d5768670ccbd25944.

[23] M. Migliorati, L. Palumbo, C. Zannini, N. Biancacci, and V. G. Vaccaro, Resistive wall impedance in elliptical multilayer vacuum chambers, Phys. Rev. Accel. Beams **22**, 121001 (2019).

[24] A. Chao, *Physics of Collective Beam Instabilities in High Energy Accelerators*, 1st ed., Wiley Series in Beam Physics and Accelerator Technology (Wiley, New York, 1993).

[25] K. Y. Ng, *Physics of Intensity Dependent Beam Instabilities* (World Scientific, Singapore, 2005).

[26] V. Smaluk, Impedance computations and beam-based measurements: A problem of discrepancy, Nucl. Instrum. Methods Phys. Res., Sect. A **888**, 22 (2018).

[27] T. He and Z. Bai, Graphics-processing-unit-accelerated simulation for longitudinal beam dynamics of arbitrary bunch trains in electron storage rings, Phys. Rev. Accel. Beams **24**, 104401 (2021).

[28] J. Calvey and M. Borland, Simulation of incoherent ion effects in electron storage rings, Phys. Rev. Accel. Beams **24**, 124401 (2021).

[29] User's Manual for ELEGANT, http://ops.aps.anl.gov/manuals/elegant_latest/elegant.html.

[30] T. He, W. Li, Z. Bai, and L. Wang, Longitudinal equilibrium density distribution of arbitrary filled bunches in presence of a passive harmonic cavity and the short range wakefield, Phys. Rev. Accel. Beams **24**, 044401 (2021).

[31] T. He, W. Li, Z. Bai, and L. Wang, Periodic transient beam loading effect with passive harmonic cavities in electron storage rings, Phys. Rev. Accel. Beams **25**, 024401 (2022).

[32] G. Skripka, A. Andersson, F. Cullinan, R. Nagaoka, and P. Tavares, Impedance characterization and collective effects in the MAX IV 3 GeV ring, in *Proceedings of the North American Particle Accelerator Conference, NAPAC2016, Chicago, IL* (CERN, Geneva, Switzerland, 2016), WEA3CO04.

[33] M. Brosi, A. Andersson, J. Breunlin, F. Cullinan, and P. Fernandes Tavares, Time-resolved measurement and simulation of a longitudinal single-bunch instability at the MAX IV 3 GeV ring, in *Proceedings of 14th International Particle Accelerator Conference, IPAC2023, Venice, Italy* (JACoW, Geneva, Switzerland, 2023), WEPA020.

[34] S. Wang, B. Zhu, Y. Gao, X. Shu, W. Wei, W. Zhang, and Y. Wang, On the synergy manipulation between the activation temperature, surface resistance and secondary electron yield of NEG thin films, Appl. Surf. Sci. **578**, 152101 (2022).

[35] T. Agoh and K. Yokoya, Calculation of coherent synchrotron radiation using mesh, Phys. Rev. ST Accel. Beams **7**, 054403 (2004).

[36] E. Roussel, C. Evain, C. Szwaj, and S. Bielawski, Microbunching instability in storage rings: Link between phase-space structure and terahertz coherent synchrotron radiation radio-frequency spectra, Phys. Rev. ST Accel. Beams **17**, 010701 (2014).

[37] C. Evain, E. Roussel, M. Le Parquier, C. Szwaj, M.-A. Tordeux, J.-B. Brubach, L. Manceron, P. Roy, and S. Bielawski, Direct observation of spatiotemporal dynamics of short electron bunches in storage rings, Phys. Rev. Lett. **118**, 054801 (2017).

[38] P. Schönfeldt, M. Brosi, M. Schwarz, J. L. Steinmann, and A.-S. Müller, Parallelized Vlasov-Fokker-Planck solver for desktop personal computers, Phys. Rev. Accel. Beams **20**, 030704 (2017).

[39] R. R. Lindberg, Practical theory to compute the microwave instability threshold, in *Proceedings of the Nonlinear Dynamics and Collective Effects in Particle Beam Physics NOCE 2017 Workshop, Arcidosso, Italy* (World Scientific, Singapore, 2019), pp. 138–146.